ELSEVIER

Polymer 42 (2001) 9705–9711

polymer

www.elsevier.com/locate/polymer

Synthesis methods of fluorinated polyurethanes. 2. Effects on morphology and microstructure

Claudio Tonelli[a,*], Giuseppe Ajroldi[a], Antonio Marigo[b], Carla Marega[b], Antonio Turturro[c]

[a]*Ausimont S.p.A., Research and Development Center, V. le Lombardia 20, I-20021 Bollate, Italy*
[b]*Dipartimento di Chimica Inorganica, Metallorganica e Analitica dell'Università, via Loredan, 4, I-35131 Padova, Italy*
[c]*Dipartimento di Chimica e Chimica Industriale dell'Università, via Dodecaneso 31, I-16146 Genova, Italy*

Received 5 April 2001; received in revised form 17 May 2001; accepted 12 July 2001

Abstract

A series of fluorinated polyurethanes, characterized by a segmented structure containing hard segments based on 4,4′-methylenebis-(phenylisocyanate) (MDI) and 1,4-butandiol (BDO), were analyzed by small- and wide-angle X-ray scattering and transmission electron microscopy (TEM) in order to study the influence of the synthesis and of the soft and hard segments length on the structure.

Theoretical models of lamellar morphology were used to fit calculated small-angle scattering patterns to the experimental ones.

TEM and small-angle X-ray scattering analysis shows that these polymers are characterized by a heterogeneous structure, not only at the molecular level, but also at a macroscopic scale. © 2001 Published by Elsevier Science Ltd.

Keywords: Fluorinated polyurethanes; X-ray scattering; Morphology

1. Introduction

Fluorinated polyurethanes (FPU) are a class of new materials which have outstanding properties in terms of mechanical and surface characteristics, and chemical resistance. They can be prepared from diisocyanates, 1ike 4,4′-methylenebis(phenylisocyanate) (MDI), chain-extenders, and macrodiols of general structure:

$$HO–R_h–R_f–R_h\ OH$$

where $R_h = –CH_2–$, $–CH_2(OCH_2CH_2)_n$ $(n = 1, 2)$, and $R_f = –CF_2O(CF_2CF_2O)_p(CF_2O)_qCF_2–$.

The central fluorinated block has the copolymeric structure of the perfluoropolyether class, which is obtained by photosynthesis from tetrafluoroethylene and oxygen at low temperature [1–3]. The perfluoropolyetheric segment is characterized by a very low glass transition temperature T_g (about −120°C for a polymer of infinite molecu1ar weight and with a p/q ratio of 1). It as been shown that T_g is a function of the O/C ratio, decreasing with increasing the oxygen content [4]. The soft fluorinated and the hard segments are not compatible, so that phase segregation occurs, as we have observed in a previous paper about the FPU morpho1ogy [5].

In a previous paper, the authors [6] studied the influence of the synthesis and of the soft and hard segment length on the structure, as determined by calorimetry and dynamic mechanical analysis; the following structures were considered:

$$–(Z–MBM)_n–\qquad \text{(structure S1)}$$

$$–[Z–M(BM)_2]_n–\qquad \text{(structure S2)}$$

$$–[Z–M(BM)_m]_n–\qquad \text{(structure SS)}$$

where Z is the $–O–R_h–R_f–R_h–O–$ soft segment, M is a diisocyanate and B is the chain-extender. While in the first two cases, the length of the hard segment is well defined, within the synthesis limits, in the last case the hard segment length is statistically distributed.

The aim of the present work is to study the structure and the morphology of the same polymers by small (SAXS) and wide-angle X-ray scattering (WAXS) and transmission electron microscopy (TEM).

Koberstein and Stein [7] suggested a lamellar model of the polyurethanes hard phase, which takes into account the folding of the hard segments; in the present work, the SAXS patterns of the studied samples are compared with

* Corresponding author. Tel.: +39-02-3835-6485; fax: +39-02-3835-2152.

E-mail address: claudio.tonelli@ausimont.com (C. Tonelli).

0032-3861/01/$ - see front matter © 2001 Published by Elsevier Science Ltd.
PII: S0032-3861(01)00517-1

Table 1
Weight, volume fraction and density of the samples

Sample	w_h	Φ_h	Density (g/cm^3)
S1-2000	0.203	0.243	1.634
S1-3100	0.137	0.174	1.711
S1-3800	0.119	0.153	1.732
S2-2000	0.276	0.326	1.583
S2-3100	0.200	0.248	1.685
SS-1000	0.286	0.337	1.594
SS-2000	0.205	0.251	1.657
SS-3100	0.156	0.197	1.700
SS-3800	0.130	0.166	1.721

calculated patterns obtained from theoretical models of lamellar thicknesses distributions.

Furthermore, the thickness of the transition layer E between the hard and the soft regions and the electron density difference between the two phases have been evaluated, together with the electron density difference between the two phases.

2. Experimental

2.1. Synthesis of materiaIs

The macrodiols used to synthesize the FPUs investigated in the present study are represented by the following structure:

$$HO(CH_2CH_2O)_nCH_2CF_2O(CF_2CF_2O)_p$$

$$\times(CF_2O)_qCF_2CH_2(OCH_2CH_2)_nOH$$

According to the above structure, these fluorinated building-blocks (produced by Ausimont S.p.A., Italy under the trade name ZDOLTX®) are a mixture of oligomeric products, consisting of a random distribution of $-CF_2CF_2O-$ (C_2 unit) and $-CF_2O-$ (C_1 unit), end capped by ethoxylated units $-CH_2O(CH_2CH_2O)_nH$ (where $n = 1$ or 2).

The molecular weight range of the macromers used in this work was between 1400 and 3800 (1400 in the sample

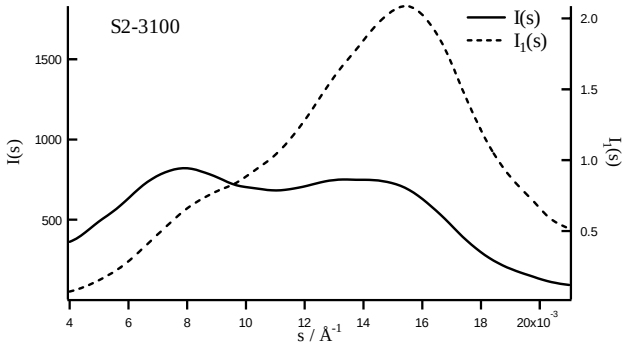

Fig. 1. Small-angle X-ray scattering function $I(s)$ and one-dimensional scattering function $I_1(s)$ of S2-3100 sample.

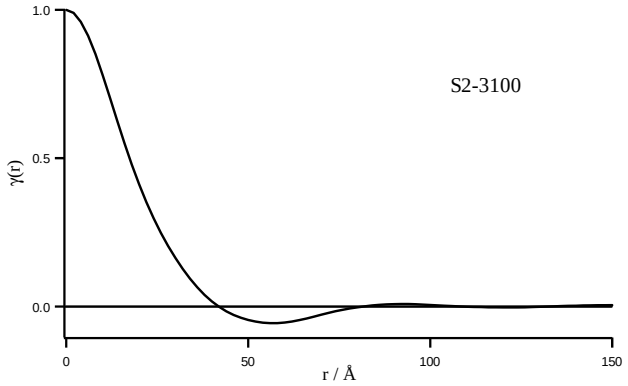

Fig. 2. Correlation function $\gamma(r)$ of S2-3100 sample.

SS-1000, 2200 in the samples S1-, S2- and SS-2000, 3100 in the samples S1-, S2- and SS-3100, 3800 in the samples S1- and SS-3800).

Other compositional and physical characteristics of the macromers and the details of the FPUs synthesis are reported in Ref. [6], while the weight and volume fractions of the hard phase in the three sets of the studied samples are reported in Table 1 together with the density of the samples determined at 23°C following ASTM D 792.

2.2. Wide-angle X-ray scattering

WAXS patterns were recorded by a powder diffractometer Seifert MZ III, equipped with a graphite monochromator on the diffracted beam, in the angular range $2\vartheta = 10$–$60°$, steps of 0.1° (2ϑ) and 10 s of recording time for each step. CuK_α X-radiation was employed.

2.3. Small-angle X-ray scattering

SAXS patterns were recorded by a Kratky camera, using the CuK_α X-radiation. The intensity data were collected by a position-sensitive detector MBraun OED-50M in the angular range 0.1–5° (2θ) and were successively corrected for the blank scattering.

The data were analyzed by the Vonk's [8] computer program and they were transformed into absolute intensity by the secondary standard method [9]. A constant continuous background scattering was then subtracted [10] and the obtained intensity values $I(s)$ were smoothed in the tail region, with the aid of the $sI(s)$ vs. $1/s^2$ plot [11], being $s = (2/\lambda)\sin\theta$.

The one-dimensional $\gamma_1(x)$ [12] and three-dimensional $\gamma(r)$ [13] correlation functions were evaluated from the smeared intensity $I(s)$. Finally, the Vonk's desmearing procedure [14] was applied and the one-dimensional scattering function was obtained by the Lorentz correction $I_1(s) = 4\pi s^2 I(s)$, where $I_1(s)$ is the one-dimensional scattering function and $I(s)$ is the desmeared intensity function.

Fig. 1 shows, as an example, the scattering functions $I(s)$ and $I_1(s)$ of the S2-3100 sample.

The use of the Lorentz correction is justified by the

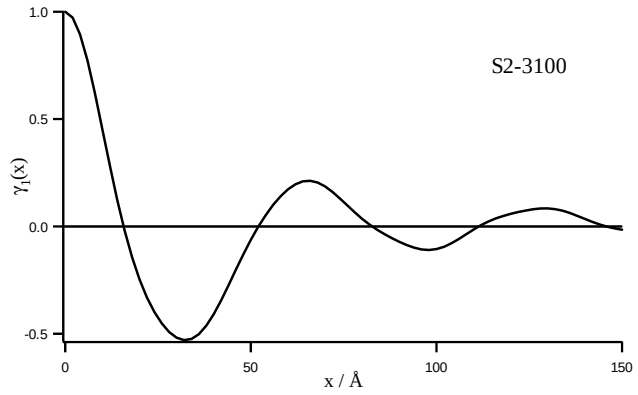

Fig. 3. One-dimensional correlation function $\gamma_1(x)$ of S2-3100 sample.

analysis of the correlation functions, which are reported, for the same sample in Figs. 2 and 3. The structure of the material is not completely random, because, in such a case, the three-dimensional correlation function would have an exponential shape [15]. Furthermore, the one-dimensional correlation function displays periodicity, indicating that the two-phase structure can be described as alternating layers of soft and hard segments [15]. A lamellar morphology was then supposed and the one-dimensional scattering functions $I_1(s)$ were compared with those calculated from theoretical models of lamellar thickness distribution, by the methods described below.

The thickness of the transition layer E between the hard and the soft regions was evaluated according to the procedure described by Vonk [11].

The electron density difference between the two phases $(\rho_h - \rho_s)$ and the inner surface S/V were calculated from the equations [12]

$$2\pi \int_0^\infty s\tilde{I}(s)\mathrm{d}s = \left[\Phi_h \Phi_s - \frac{E}{6}\frac{S}{V} \right](\rho_h - \rho_s) \tag{1}$$

$$\frac{4}{\pi} \frac{\lim_{s\to\infty} s^3\tilde{I}(s)}{\int_0^\infty s\tilde{I}(s)\mathrm{d}s} = \frac{\left(\frac{S}{V}\right)(\rho_h - \rho_s)}{2\pi^2 \Phi_h \Phi_s} \tag{2}$$

where Φ_h and Φ_s are the volume fractions of the hard and soft phases.

Finally, the inhomogeneity length l_p was evaluated by [16]

$$I_p = \frac{4\Phi_h\Phi_s}{\frac{S}{V}} \tag{3}$$

and the average length of the segments lying within the hard and soft phases were obtained from $l_h = l_p/\Phi_s$ and $l_s = l_p/\Phi_h$.

2.3.1. Theoretical evaluation of the SAXS patterns

The intensity profile of the SAXS patterns, according to some theoretical distribution models [17,18], was evaluated as [19]

$$I(s) = I'(s) + I''(s) \tag{4}$$

where

$$I'(s) = \frac{(\rho_h - \rho_s)^2}{4\pi^2 s^2 D} \frac{|1 - F_h|^2(1 - |F_s|^2) + |1 - F_s|^2(1 - |F_h|^2)}{|1 - F_h F_s|^2} \tag{5}$$

$$I''(s) = \frac{(\rho_h - \rho_s)^2}{2\pi^2 s^2 DN} \mathrm{Re}\left\{ \frac{F_s(1 - F_h)^2(1 - (F_s F_h)^N}{(1 - F_s F_h)^2} \right\} \tag{6}$$

In these equations, F_h and F_s represent the Fourier transforms of the Gaussian distribution functions of the hard and soft phases regions thicknesses (H and S), ρ_h and ρ_s are the electron densities of the hard and soft regions, respectively, N is the number of the lamellae in the stack and D the average long period.

The optimized parameters were the average hard region thickness H, the Gaussian distribution standard deviation of the thickness σ_h, $\Phi_h = H/D$ and N, while the average thickness of the soft regions $S = [(1 - \Phi_h)/\Phi_h]H$ and its Gaussian distribution standard deviation $\sigma_s = (\sigma_h/H)S$.

2.4. Transmission electron microscopy

TEM was performed on samples stained by exposure of the bulk specimen and of the ultrathin sections to vapors of 0.5% aqueous solution of ruthenium tetroxide, RuO_4, for 30 min. More details about the staining procedure of such samples are reported in a previous work [5]. Ultrathin sections of about 800 Å were ultramicrotomed at −130°C with a Reichert Ultramicrotome model OM-U2, equipped with a diamond knife at −80°C. They were observed by means of a Siemens Elmiskop 1101 transmission electron microscope under an acceleration voltage of 100 kV.

3. Results and discussion

3.1. Wide-angle X-ray scattering

Fig. 4 reports the WAXS pattern of the S2-3100 sample,

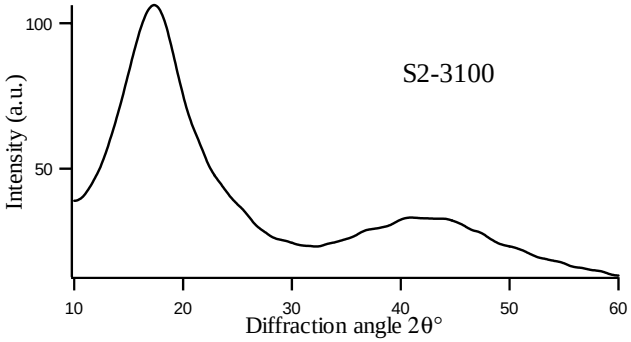

Fig. 4. Wide-angle X-ray scattering pattern of S2-3100 sample.

Table 2
SAXS parameters: electron density difference between the hard and soft phases ($\rho_h - \rho_s$), transition layer thickness E and average length of the segments lying in the hard (l_h) and soft (l_s) phases

Sample	$(\rho_h - \rho_s)$ (mol electr./cm^3)	E (Å)	l_h (Å)	l_s (Å)
S1-2000	0.34	9	34	106
S1-3100	0.20	7	25	122
S1-3800	0.21	7	26	149
S2-2000	0.23	4	55	113
S2-3100	0.18	8	30	92
SS-1000	0.24	7	20	40
SS-2000	0.23	6	32	95
SS-3100	0.16	6	33	137
SS-3800	0.22	8	15	75

but all the samples show a similar behavior: there is no evidence of sharp peaks in the patterns and this can be related to the absence or to smallness of crystalline regions in the hard phase.

3.2. Small-angle X-ray scattering

The SAXS functions $I(s)$ and $I_1(s)$ of the S2-3100 sample (Fig. 1) show two partially overlapped peaks and such a phenomenon, which occurs in all the examined samples, even if it is more evident in the S2 set, is related to the presence of regions with bimodal distribution of the long period thicknesses.

In spite of this experimental evidence, the evaluation of parameters such as the electron density difference $(\rho_h - \rho_s)$, the average lengths l_h and l_s of the segments lying within the hard and soft phases and the transition layer thickness E, can be useful even if they only give information about the average thickness of the phases. The obtained data are reported in Table 2.

With the exceptions of sample S2-2000, which differs for the lowest value of E and the highest value of l_h, and of sample SS-3800, which shows the lowest value of l_h, the average length of the hard phase l_h and the transition layer thickness do not remarkably change. The electron density

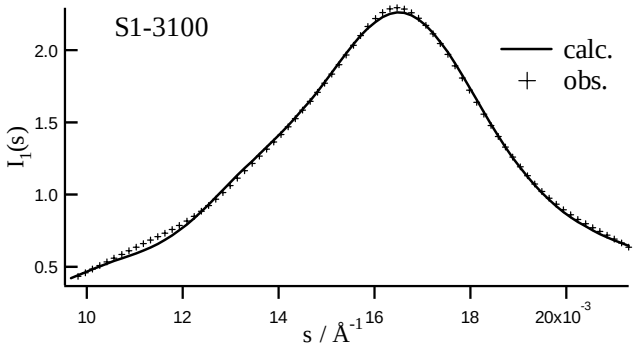

Fig. 5. Best fit between experimental and calculated small-angle one-dimensional scattering functions of S1-3100 sample.

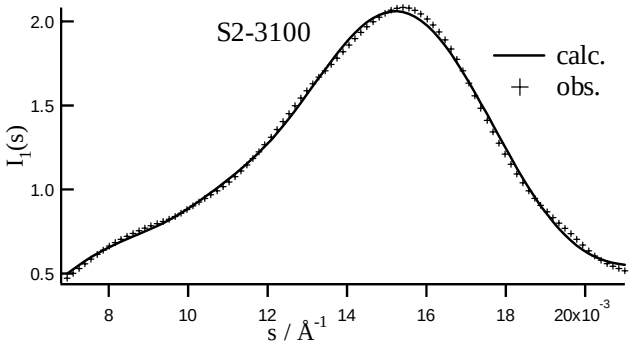

Fig. 6. Best fit between experimental and calculated small-angle one-dimensional scattering functions of S2-3100 sample.

difference $(\rho_h - \rho_s)$, with the exception of the samples S1- and SS-3800, decreases with increasing of the ZDOLTX molecular weight because of, probably, an increase of the two phases mixing. This could be due to an increase of melt viscosity of the system, which slows down the phase separation predicted by thermodynamic requirements.

All these data are to be considered as an average of all the lamellar stackings in the samples while the above-described fitting procedure allows an independent evaluation of the two overlapped peaks in the SAXS patterns.

Figs. 5–7 show the best fits obtained, for ZDOLTX 3100 based materials, by comparing the experimental one-dimensional scattering functions with patterns calculated from Gaussian distribution models. Table 3 reports the optimized parameters of lamellar thickness, relative dispersion of thickness and hard phase volume fraction for all polymers. The subscript numbers point out that two different populations of lamellae have been introduced in the calculation: the number 1 is related to the stacking having larger long-period. The hard phase volume fraction Φ_h values are common to the different populations in each sample.

Some considerations on the samples morphology can be made from the data of Table 3.

The SS samples show a hard phase thickness comparable with those of the other sets, in spite of the fact that the statistical synthesis should introduce a growth of the hard segment.

A first interpretation of this phenomenon could be

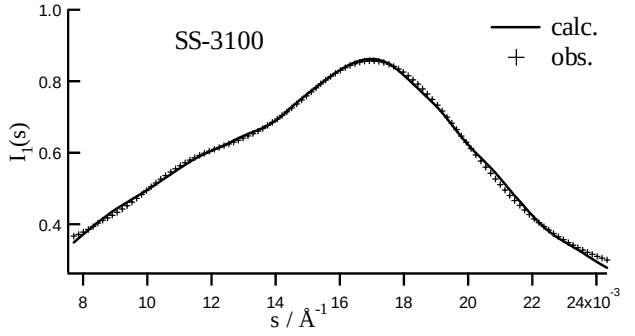

Fig. 7. Best fit between experimental and calculated small-angle one-dimensional scattering functions of SS-3100 sample.

Table 3
SAXS parameters from the fitting procedure: average thickness of the hard (H) and soft (S) phase regions and long period D; relative dispersion of the hard phase region thickness σ_H/H and hard phase fraction Φ_h

Sample	H_1 (Å)	S_1 (Å)	D_1 (Å)	$(\sigma_H/H)_1$	H_2 (Å)	S_2 (Å)	D_2 (Å)	$(\sigma_H/H)_2$	Φ_h
S1-2000	13	40	53	0.42	–	–	–	–	0.23
S1-3100	13	61	74	0.31	10	48	58	0.20	0.17
S1-3800	16	90	106	0.50	10	53	63	0.20	0.15
S2-2000	23	53	76	0.17	20	47	67	0.30	0.30
S2-3100	17	63	80	0.35	13	51	64	0.08	0.21
SS-1000	14	67	81	0.28	11	50	61	0.36	0.18
SS-2000	–	–	–	–	13	55	68	0.46	0.19
SS-3100	17	72	89	0.53	12	49	61	0.33	0.20
SS-3800	16	80	96	0.56	9	46	55	0.33	0.16

founded in a larger distribution of hard phase thickness around to average values comparable to those of the other sets (see the larger values of σ_h/H in SS set), as well as in possible presence of chain folding [7].

As concerns the soft phase, the thickness of population 1 (S_1) increases in all the sets with increasing of the ZDOLTX molecular weight.

A common characteristic of the samples is the presence of a second population which shows a smaller long period and whose soft phase thickness have only slight fluctuations around the value of 50 Å.

Such behavior inclines to suppose the presence of soft phases with different molecular weights, which organize in separate domains.

The hard phase volume fraction, evaluated by the fitting procedure, decreases with increasing of the ZDOLTX molecular weight in the S1 and S2 sets, while it slightly fluctuates in SS. Furthermore, the relative dispersion of the lamellar thicknesses is generally larger in the last set than in the other series and this agrees with the statistical synthesis of the SS set.

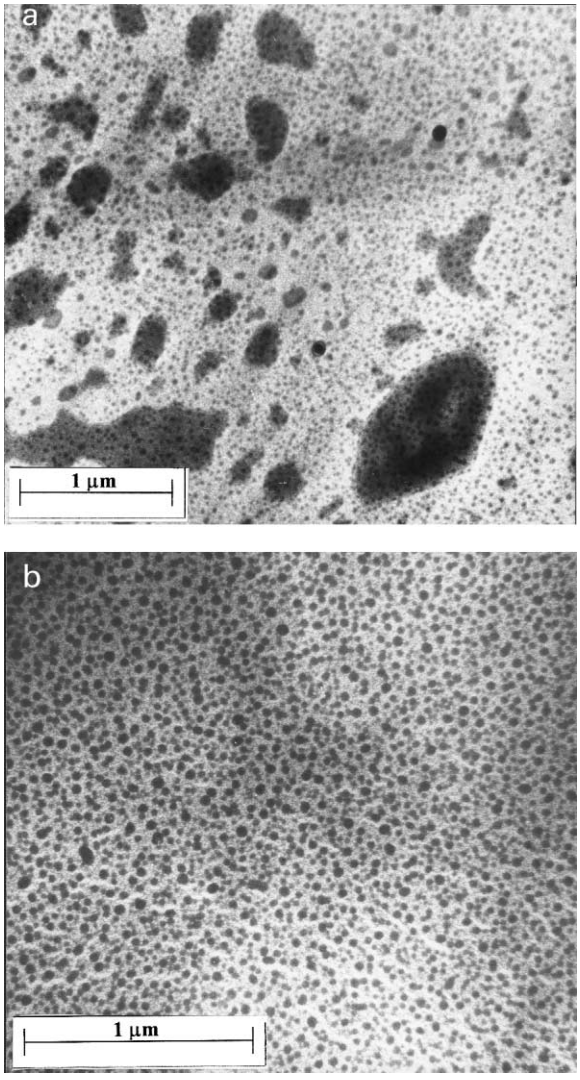

Fig. 8. TEM of S1-2000 FPU, stained with RuO_4; (a) and (b) are different regions of the same sample.

4. Morphology

As shown elsewhere [5], RuO_4 is an effective staining agent to discriminate the fluorinated phase from the hydrogenated one of such polymers. In fact, RuO_4 is a strong oxidizing agent of a variety of chemical groups present in polymers [20,21], like aromatic rings and ethers. Perfluorinated chains do not react with it, even after several hours of exposure to its vapor.

Therefore, in the following TEM micrographs, hard phase domains are dark while the soft fluorinated phase remains white.

Fig. 8a,b is a TEM micrograph of S1-2000 copolymer. It shows a wide size distribution of dark phase microdomains, with aggregate size ranging from 0.03 to 1.5 μm (Fig. 8a), dispersed in a white soft segment matrix. The apparent bigger domains are grey and not deep dark, like the smaller ones, and contain darker subdomains of about 0.03 μm size. We deem that they are not made of pure hard blocks; they could be simply indicative of matrix zones with a lower soft segment concentration. Moreover, there are zones where only small dark microdomains, always of about 0.03 μm size, are present with a sharp size distribution (Fig. 8b).

The same morphology is observed for S1-3100 and S1-3800

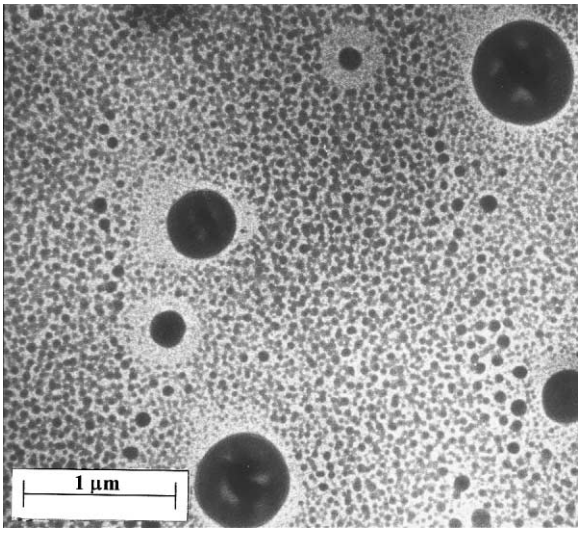

Fig. 9. TEM micrographs of ultrathin sections of S2-3100 FPU stained with RuO_4.

copolymers. In the last case, however, the extent of segregation is lower than in the first two copolymers.

Copolymers of S2 series exhibit the same morphology of aforementioned copolymers, with dark small and big domains (0.04–0.7 μm) of hard phase in the white fluorinated matrix (Fig. 9). However, some main characteristics mark them: the big domains are always spherical-shaped and contain white subdomains of fluorinated material; moreover, around them the matrix is hard phase poorer than other zones. All this suggests a higher incompatibility between fluorinated and hydrogenated blocks as well as stronger interactions among hard segments, owing its their longer sequences, than occurs in S1 series.

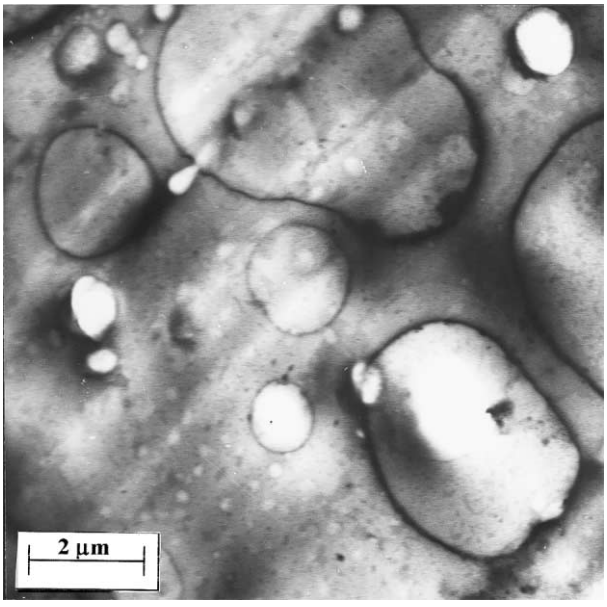

Fig. 10. TEM micrographs of ultrathin sections of SS-1000 FPU stained with RuO_4.

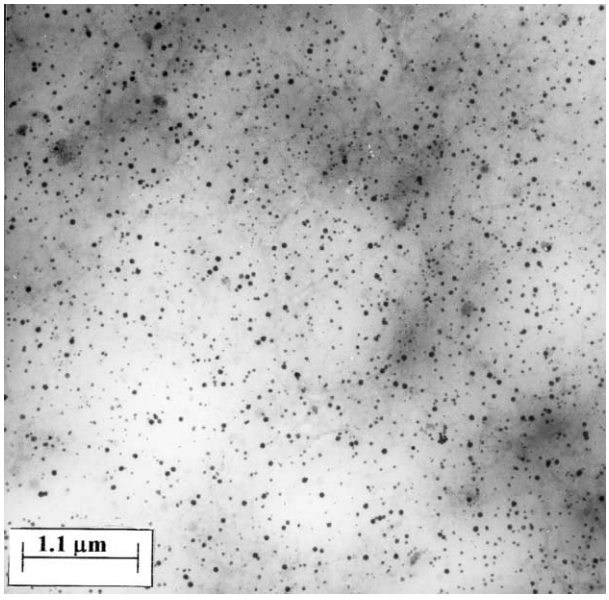

Fig. 11. TEM micrographs of ultrathin sections of SS-2000 FPU stained with RuO_4.

SS copolymers, which were synthesized with the same Z/M/B (1/2/1) ratio as for S1 series but following standard method, should give rise to a wider distribution of hard segment sequence lengths. As a matter of fact, morphologies of the three SS copolymers are different among them and from those of S1 series.

The morphology of SS-1000 copolymer exhibits (Fig. 10) white macrodomains of hard segments (up to about 5 μm), more or less spherical-shaped, with a black contour, dispersed in a grey matrix also containing white (0.1–0.5 μm) and very small dark subdomains (0.03–0.5 μm). This morphology seems to be due to a co-continuous distribution both of the components, as suggested by Chen et al. [22].

The SS-2000 copolymer has the same composition of S1-2000, with $w_h = 0.205$; however, its morphology is characterized by a wide size distribution of hard domains of about 0.05–3 μm in diameter and a heterogeneous dispersion of macrodomains of hard segments, which is not found in the case of S1-2000 copolymer. The micrograph of Fig. 11 shows only dark microdomains (less than 0.05 μm in diameter) of hard phase in a partially grey matrix. This one could be formed by a dispersion of short hard blocks and/or very small hard domains in a fluorinated soft segment phase, as suggested by SAXS data.

A comparison between SS-2000 and S1-2000 morphologies puts into evidence that in the first case a lower number of hard phase microdomains is visible, probably due to the segregation in the aforementioned macrodomains, as a consequence of hard blocks with different chain lengths present in the standard polymer.

Fig. 12 refers to the morphology of SS-3100 copolymer. It shows a very different morphology from those of previous copolymers, without macrodomains of hard segments. It

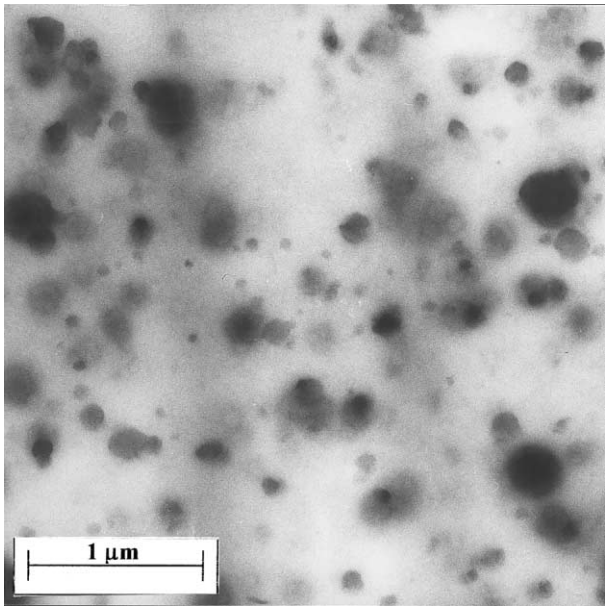

Fig. 12. TEM micrographs of ultrathin sections of SS-3100 FPU stained with RuO_4.

exhibits a wide size distribution of hard segment domains, from 0.05 to 0.5 μ in diameter, dispersed in the fluorinated soft matrix, which is slightly grey for the same reasons before discussed.

5. Concluding remarks

The SAXS data confirm that always two phases of soft and hard segments are found because of the low compatibility between the two kind of segments, as concluded in Ref. [6] from thermal and dynamic-mechanical analysis.

The comparison of SAXS and TEM data shows that these polymers are characterized by a heterogeneous structure, not only at the molecular level, but also at a macroscopic scale. The presence of two families of structures found by SAXS analysis, one dependent and the other one nearly independent on the molecular weight of the soft segment, could be tentatively explained either by the non quantitative structural yield obtained through the so-called 'regular synthesis', or by a reality in some a way different from the structural model used.

The second kind of heterogeneity, i.e. that observed by TEM analysis, could be possibly due to the polymerization condition. TEM analysis shows indeed that the dispersed hard phase is constituted by domains or clusters in which a fraction of soft segments is dispersed; their size and fraction are dependent on the polymerization procedure. The macrostructure is more regular, as expected, for polymers prepared by S1 and S2 synthesis.

Comparison of SAXS and WAXS data suggests that crystalline domains are very small; the large amplitude of the WAXS main peak points out that the lateral order is lost at very short distance.

References

[1] Sianesi D, Pasetti A, Fontanelli R, Bernardi GC, Caporiccio G. Chim Ind, Milan 1973;55(I):208–21.
[2] Faucitano A, Buttafava B, Martinotti F, Marchionni G, Staccione A, De Pasquale RJ. ACS Ninth Winter Fluorine Conference, St Petersburg (FL), USA. 1998. p. 52.
[3] Faucitano A, Buttafava B, Guarda PA, Marchionni G. Third International Conference On Polymer Photochemistry, Sestri Levante, Italy. 1993. p. 178.
[4] Marchionni G, Ajroldi G, Cinquina P, Tampellini E, Pezzin G. Polym Engng Sci 1990;30:829–34.
[5] Gattiglia EG, Turturro A, Tonelli C, Trombetta T, Ajroldi G. Int J Polym Anal Charact 1998;4:295–308.
[6] Tonelli C, Ajroldi G, Turturro A, Marigo A. Polymer 2001;42:5589–98.
[7] Koberstein JT, Stein RS. J Polym Sci, Polym Phys 1983;21:1439–72.
[8] Vonk CG. J Appl Crystallogr 1975;8:340–1.
[9] Krayky O, Pilz I, Schmidt PJ. J Colloid Interf Sci 1966;21:24–34.
[10] Vonk CG, Pijpers AP. J Polym Sci, Polym Phys 1985;23:2517–37.
[11] Vonk CG. J Appl Crystallogr 1973;6:81–6.
[12] Vonk CG. In: Glatter O, Kratky O, editors. Synthetic polymers in the solid state in small angle X-ray scattering. London: Academic Press, 1982. Part 13.
[13] Porod G. In: Glatter O, Kratky O, editors. General theory in small angle X-ray scattering. London: Academic Press, 1982. Part 2.
[14] Vonk CG. J Appl Crystallogr 1971;4:340–2.
[15] Ophir Z. J Polym Sci, Polym Phys 1980;18:1469–80.
[16] Ruland W. J Appl Crystallogr 1971;4:70–3.
[17] Marega C, Marigo A, Cingano G, Zannetti R, Paganetto G. Polymer 1996;37:5549–57.
[18] Blundell DJ. Polymer 1978;19:1258–66.
[19] Hosemann R, Bagchi SN. Direct analysis of diffraction by matter. Amsterdam: North Holland, 1962.
[20] Trent JS, Schebeim JI, Couchman PR. J Polym Sci, Polym Lett 1981;19:315–9.
[21] Trent JS, Schebeim JI, Couchman PR. Macromolecules 1983;16:589–98.
[22] Chen CHY, Briber RM, Thomas EL, Xu M, Mac Knight WJ. Polymer 1983;24:1333–40.